Journal of Zhejiang University-SCIENCE A (Applied Physics & Engineering)
ISSN 1673-565X (Print); ISSN 1862-1775 (Online)
www.jzus.zju.edu.cn; www.springerlink.com
E-mail: jzus@zju.edu.cn

Methodology for expressing the flow coefficients of coupled throttling grooves in a proportional–directional valve*

Xiao-lu ZHANG[1], An-lin WANG[1], Wei CHEN[2], Long KUANG[1], Tao JIANG[†‡1]

[1]*School of Mechanical Engineering, Tongji University, Shanghai 201804, China*

[2]*Guizhou Jonyang Kinetics Co., Ltd., Guiyang 550006, China*

[†]E-mail: jiangtao@tongji.edu.cn

Received Dec. 24, 2019; Revision accepted July 28, 2020; Crosschecked Sept. 16, 2020

Abstract: Calculating the flow coefficient of a spool-valve is complicated due to the coupling–throttling effect in the throttling grooves of a proportional–directional valve. In this paper, a methodology for expressing the flow coefficient of coupled throttling grooves is proposed to resolve that difficulty. With this purpose, an approach of a 3D numerical simulation and an experimental bench were introduced based on the prototype of a commercial proportional valve. The results show consistency between the numerical simulation and the bench test. Based on that, the concept of 'saturation limit' is introduced to describe the value gap between the current and saturated flows, so that the flow-coefficient saturation limit of the prototype in the process can be deducted. Accordingly, an approximate flow coefficient suitable for coupled throttling grooves within finite variable space, which is based on three typical throttling structures (i.e. O-shape, U-shape, and C-shape) of the coupled throttling grooves, is obtained based on an orthogonal test. The model results are consistent with the numerical and experimental results, with maximum errors of less than 5.29% and 5.34%, respectively. This suggests that the proposed method is effective in approximating the flow coefficient.

Key words: Flow coefficient; Proportional–directional valve; Coupled throttling grooves; Saturated flow
https://doi.org/10.1631/jzus.A1900656 **CLC number:** TH161.12

1 Introduction

The hydraulic proportional valve is a proportional control valve in an oil circuit, which regulates the flow rate in proportion to the displacement of the spool by changing the flow area of the throttling grooves. This type of valve is widely used due to its stability and user-friendly features. Associated studies (Tamburrano et al., 2019a, 2019b) mainly focus on the following aspects: (1) flow characteristics and structural optimization from a fluid-dynamic perspective; (2) approaches of simulation and test for a spool valve. With respect to the first aspect, several central issues have been studied. The fluid flow through hydraulic valves was studied with the method of 3D computational fluid dynamics (CFD) analysis (Lisowski and Rajda, 2013; Amirante et al., 2014c; Wu et al., 2015; Lisowski and Filo, 2016), and optimizations of spool and housing geometries were also conducted (Simic and Herakovic, 2015; Frosina et al., 2018). Amirante et al. (2006, 2014b, 2016) proposed an effective methodology for optimizing the sliding spool of a hydraulic proportional–directional valve by numerically analyzing the driving forces acting on the valve spool. Meanwhile, the effect of cavitation on the performance of hydraulic spool valves was investigated (Chattopadhyay et al., 2012; Amirante et al., 2014a; Okabe et al., 2019). Fu et al. (2008) found the characteristics of the distribution of cavitation in

‡ Corresponding author

* Project supported by the National Key R&D Program of China (No. 2018YFC0810203)

ORCID: Xiao-lu ZHANG, https://orcid.org/0000-0003-3799-9244; Tao JIANG, https://orcid.org/0000-0002-2715-294X

valves with different grooves. Jin et al. (2020) studied the effect of valve core shapes on cavitation flow through a sleeve regulating valve. The second aspect focuses on the approaches of simulation and test. Using numerical methods, Srikanth and Bhasker (2009) and Zalogin et al. (2018) investigated the flow field in a spool valve by moving-grid technology, and Borghi et al. (1998) performed a commercial CFD code in order to reduce the computational work. Palau-Salvador et al. (2008) illustrated the importance of full 3D geometry effects in modelling and optimizing control valve performance in CFD modelling. Frosina et al. (2017) introduced a 3D CFD modelling approach verified on a two-way pressure-compensated flow control valve. A spool-type pressure-regulating valve was studied using the direct CFD approach and suggested that the standard k–ε model of turbulence can predict high levels of turbulent kinetic energy, and that the realizable variant of the k–ε model should be adopted for turbulence closure (Chattopadhyay et al., 2012). Chen et al. (2018) proposed a method for optimization of spool valve flow force based on the MATLAB-AMESim-Fluent joint simulation method. Meanwhile, with respect to the test facility, Majdič et al. (2011) built an experimental facility to investigate the lifetime performance of a proportional 4/3 hydraulic valve operating in water. The test facility has also been mentioned in many studies (SAE, 2017; Lu et al., 2019). From the literature cited, it is obvious that CFD and experimental methods are common in related studies.

In general, in the process of proportional spool-valve design, the flow coefficient is considered as a constant with a value between 0.61–0.67 (Hua et al., 2018). However, many researchers (Lisowski and Filo, 2016, 2017; Lisowski et al., 2018; Afatsun and Balkan, 2019) have shown that the spool-valve flow coefficient varies according to changes in the throttling boundary. Lisowski and Filo (2017) proposed three approximating functions of the flow coefficient by a curve-fitting method, all of which were related to the spool position and, to a lesser extent, to the volumetric flow rate. Valdés et al. (2014) developed a methodology based on an anti-locked braking system (ABS) valve for the parametric modelling of hydraulic-valve flow rates. Ye et al. (2014) studied three notches and their corresponding typical structural grooves by CFD and test investigations to clarify the effects on the flow characteristics. Pan et al. (2011) researched the influence of the throttling-groove structure of a spool valve on fluid characteristics in the working process by similar approaches, and established related mathematical models that reflected flow-coefficient variations in the process (mainly laminar flow). Lisowski et al. (2015) analyzed the flow characteristics of a proportional flow-control valve and optimized its characteristics by geometrically modifying the spool. Based on the 2D CFD technique, mathematical models were established that simulate the pressure and flow rate characteristics of a spool valve with variable flow coefficients through the spool-valve ports, assuming them to be functions of the Reynolds number and orifice geometry rather than constants (Afatsun and Balkan, 2019). Wang et al. (2014) derived a precise function expression for the flow area for a sloping U-shape notch orifice with respect to spool valves machined by different methods. Zhang et al. (2018) also built two artificial neural network (ANN) modes separately to express the flow coefficients of two coupled notches.

Thus, structural optimization, simulation methods, and the variation laws of the spool-valve flow rate and flow coefficient have been examined in previous studies. The studies mentioned have focused on either the structure of a single throttling groove or multiple structures without considering the effect of different coupled structures with different shapes. Thus, the applicability of the relevant methods requires verification. More importantly, since the flow coefficient is also affected by structural variations, the mechanism behind this influence requires further investigation.

In order to address these elements, a typical proportional valve used in the swing circuits of hydraulic excavators to control the swing mechanism proportionally, is taken as an example in this study, which is carried out with different combinations of coupled throttling grooves across three typical structures (O-shape, U-shape, and C-shape). A saturation-limit model of the flow coefficient is established in the process. Firstly, the throttling characteristics of a typical valve model at different openings and flow rates are obtained using the CFD approach and a bench test. Based on earlier studies conducted by the authors (Wang et al., 2018; Zhang et al., 2018), it is clear that the working flow rate of these typical valves

is responsible for a high Reynolds number, which is generally $>10^5$. Moreover, it is clear that, in deriving the functional relationship between the flow coefficient and the Reynolds number, the influence of varying fluid-flow states can be identified, and the limit value of the flow coefficient and the saturation limit can be obtained by least-squares fitting. Accordingly, flow-coefficient variation law in the finite variable space of throttling-groove structures can be identified using the orthogonal-design approach. On this basis, an approximate expression model of the flow coefficient is established for parameter calibration and, by error analysis and sample testing, the model is proven to be highly effective. Therefore, the method is suitable for expressing the flow coefficients of a proportional–directional spool valve.

2 Throttling principle

The research subject of this study is a 6/3 proportional spool valve. The details of this valve are described in previous studies by the authors (Wang et al., 2018; Zhang et al., 2018). Indeed, the basic principle and characteristics of the objective valve can be expressed with a general mathematical model of a typical spool valve. Fig. 1 illustrates the typical structure of the valve in question. B and W are connections connected to the actuator, C and T are connections connected to the oil tank, and P–C is the bypass line of the valve.

The valve function can mainly be divided into three stages:

(1) When the valve spool is in the neutral position, the P–C opening is fully open and the oil returns to the tank through the fluid path.

(2) When the spool is sliding to the left/right, the P–B/W opening gradually opens and a small amount of oil reaches the hydraulic actuator through the fluid path; moreover, the P–C opening simultaneously closes and a small amount of the oil from the pump returns to the tank through the fluid path.

(3) When the throttling grooves for fluid path P–B/W are fully open, the P–B/W opening is also fully open and the oil from the pump reaches the actuator through the fluid path fully.

Moreover, the working process can be divided into the movement control of the valve spool and the throttling characteristics of the P–B/W opening. The kinematic equation (Lisowski et al., 2015, 2018) of the valve spool in the reversing process is as follows:

$$m\frac{\mathrm{d}^2x}{\mathrm{d}t^2}+F_{\mathrm{ss}}+F_{\mathrm{ts}}+F_{\mathrm{hd}}=F_{\mathrm{p}}, \tag{1}$$

where m is the valve-spool mass; x is the valve opening (unless otherwise stated), which equates to the valve-spool displacement here; t is the time; F_{ss} is

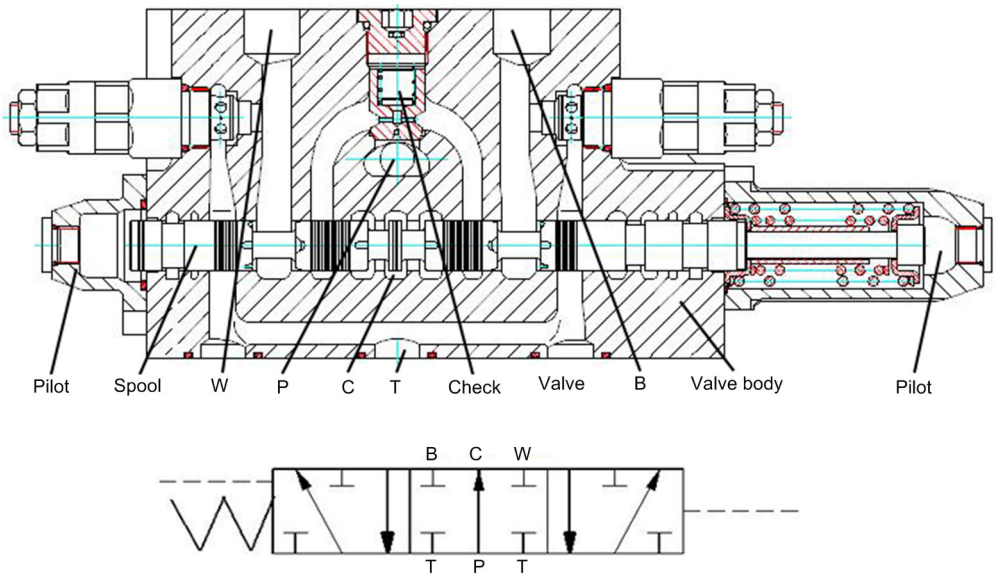

Fig. 1 Sketch of the typical geometric architecture of the valve

the spring force; F_{ts} is the viscous resistance, which is opposite to the direction of the pilot force; F_{hd} is the hydraulic force, which is near the opening; F_p is the pilot force generated by the pilot pressure. At the working phase, the throttling formula (White, 1999) is as follows:

$$Q = C_d A \sqrt{\frac{2\Delta P}{\rho}}, \tag{2}$$

where Q is the flow rate of the P–B/W flow channel; C_d is the flow coefficient; A is the flow area of the throttling groove; ΔP is the differential pressure between the inlet and outlet of the valve port; ρ is the oil density. Indeed, since A is inherently a structural parameter, it varies according to the valve opening. Moreover, the flow coefficient C_d is a comprehensive indicator of throttling at the valve port, which is determined by external working conditions and structural parameters.

The flow area can be expressed as

$$A = \Gamma(\boldsymbol{L}, x), \tag{3}$$

where $\boldsymbol{L}$ refers to the structural parameters of the throttling grooves. The expression can be obtained from the specific structure of the throttling grooves. Through theoretical derivation and programming, the exact method of which can be found in (Hong and Kim, 2016; Wang et al., 2018), the flow-area curve with respect to spool displacement is obtained, as shown in Fig. 2.

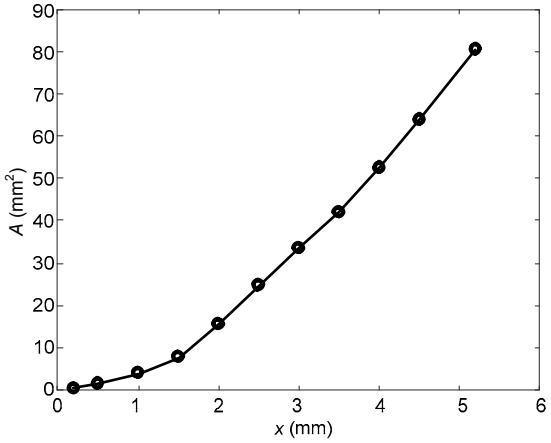

Fig. 2 Curve of flow area

Generally speaking, C_d is regarded as a constant in a number of engineering applications (Hua et al., 2018; Wang et al., 2018); however, it may vary significantly in some working environments, such as during laminar discharge (Lisowski and Filo, 2016). The conditions required to ensure a stable flow coefficient and its value are uncertain. Moreover, due to external working conditions, oil properties, and throttling structure, it is difficult to parameterise C_d (Lisowski and Filo, 2016, 2017).

3 CFD simulation and test validation

3.1 CFD simulation

In order to express the required throttling characteristics simply and explicitly, the throttling flow of a single valve port is obtained by the CFD method. The simulations are developed with a 3D numerical code Simerics PumpLinx®, developed by Simerics Inc., the USA. This tool is specially designed and contains different templates of a wide range of pumps, motors, and valves. Simerics PumpLinx is used for analyzing the fluid dynamics in the valve chamber in this study. During our simulation process, the flow is set as turbulent. In addition, a specific template of valves is used, which is based on the Reynolds-averaged Navier–Stokes equations, as well as a conventional turbulence standard k–ε model (Amirante et al., 2014c; Wu et al., 2015; Zalogin et al., 2018).

As can be seen from the physical diagram of the spool and valve body in Fig. 3, the throttling grooves consist of three fundamental structures: O-shape, U-shape, and C-shape. These structures are widely used in construction machinery since they can be processed to meet design needs. Therefore, a 3D geometric model of the fluid path P–B, as shown in Fig. 4, is created in line with the prototype valve. The throttling groove parameters of the prototype valve are shown in Table 1 (p.804). The diameter of the valve spool is 18.5 mm and the length of the valve chamber is 11.0 mm. According to Lisowski and Rajda (2013) and Vanella et al. (2014), the mesh grids must be refined based on necessary requirements with respect to complex geometry. Fig. 5 illustrates the refined mesh of fluid path P–B (taking the opening x= 2.5 mm as an example), which contains about 114 000 cells (the maximum cell size is 0.04 mm, and the minimum cell size is 0.001 mm).

With respect to the simulation settings, the constant pressure-difference method and constant-flow method can be used to determine the boundary conditions (Ye et al., 2014). Considering the working reality and bench test conditions, the constant-flow method is adopted by setting the inlet flow rate as the inlet condition and the static-pressure outlet as the outlet condition. In addition, three openings (x=2.5, 3.5, and 4.5 mm) during the opening process are selected for analysis. Fluids that are in contact with solids are defined as stationary walls (Pan et al., 2011; Frosina et al., 2018; Wang et al., 2018). The remaining details are as follows:

(1) The fluid is considered as an incompressible Newtonian fluid.

(2) The hydraulic oil density ρ is 890 kg/m^3.

(3) The kinematic viscosity of the fluid μ is 47.41 mm^2/s.

(4) The bulk modulus is 700 MPa.

(5) The outlet pressure is set to 2 MPa.

(6) Monitoring points are set near the inlet and outlet to obtain pressure data.

(7) The solution accuracy is set to 10^{-5}.

(8) The flow rates set at the inlet of the fluid path are shown in Fig. 10.

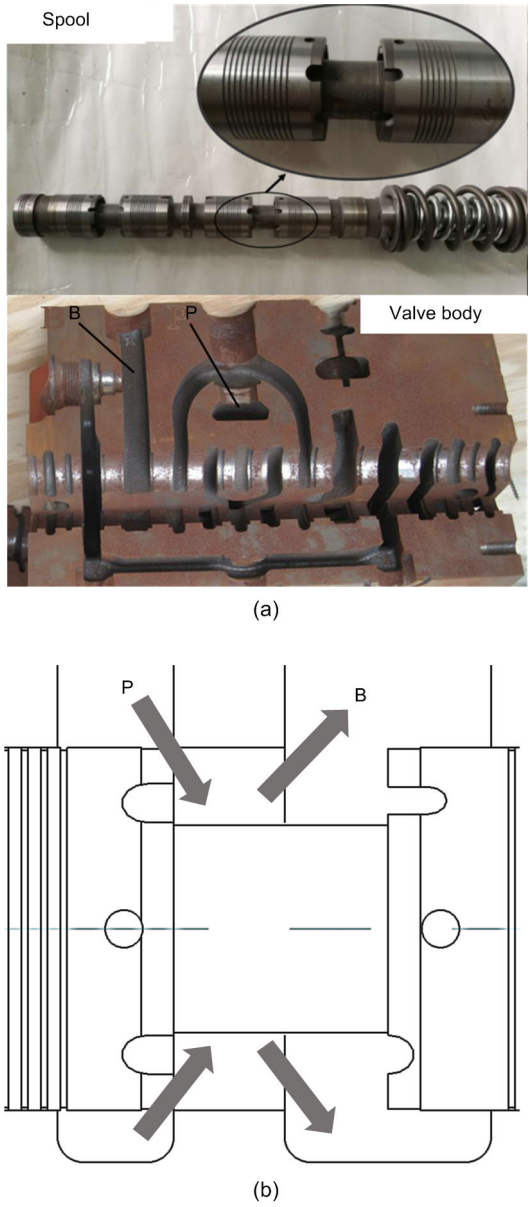

Fig. 3 Physical diagram of the prototype valve
(a) Structure of the prototype spool and valve body; (b) Sketch map of the fluid path P–B

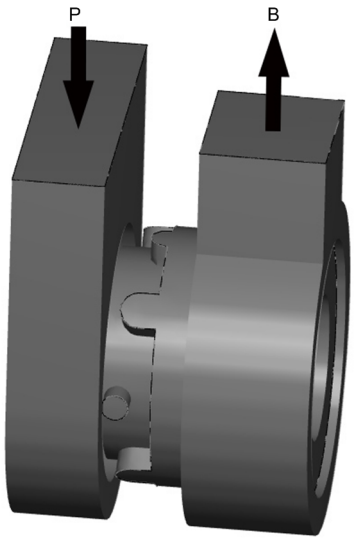

Fig. 4 3D geometric model of the fluid path P–B

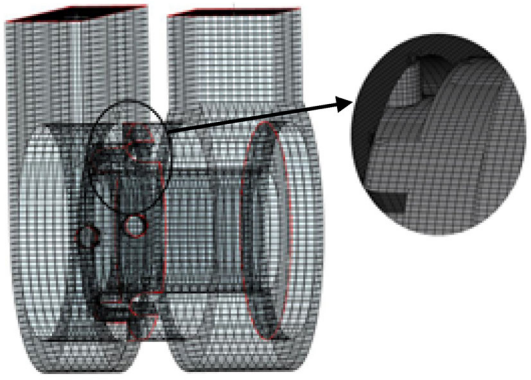

Fig. 5 Mesh diagram of fluid path P–B

3.2 Throttling test

In order to verify the effectiveness of the CFD simulation at any opening of the spool valve, a test device is built according to the sketch shown in Fig. 6.

Table 1 Orthogonal test samples and the real prototype

Sample	l_1 (mm)	l_2 (mm)	l_3 (mm)	l_4 (mm)	l_5 (mm)
1	1.6	3.2	4.6	1.2	0.9
2	1.6	3.6	4.9	1.6	1.2
3	1.6	4.0	5.2	2.0	1.5
4	1.6	4.4	5.5	2.4	1.8
5	2.0	3.2	4.9	2.0	1.8
6	2.0	3.6	4.6	2.4	1.5
7	2.0	4.0	5.5	1.2	1.2
8	2.0	4.4	5.2	1.6	0.9
9	2.4	3.2	5.2	2.4	1.2
10	2.4	3.6	5.5	2.0	0.9
11	2.4	4.0	4.6	1.6	1.8
12	2.4	4.4	4.9	1.2	1.5
13	2.8	3.2	5.5	1.6	1.5
14	2.8	3.6	5.2	1.2	1.8
15	2.8	4.0	4.9	2.4	0.9
16	2.8	4.4	4.6	2.0	1.2
Prototype	2.1	3.8	5.0	1.8	1.4

l_1–l_5 are the throttling groove parameters as shown in Fig. 13. l_1 is the radius of the C-shape structure; l_2 is the length of the U-shape structure; l_3 is the maximum of valve opening; l_4 is the radius of the U-shape structure; l_5 is the radius of the O-shape structure

L-HM 46 hydraulic oil with a nominal kinematic viscosity of 47.41 mm^2/s at 40 °C is used as the working liquid. The bench provides the measurement of inlet and outlet pressures, flow rate, accurate control of the spool position, as well as adjustment of the flow in the tested fluid path (Wang et al., 2018; Zhang et al., 2018). The test bench is mainly composed of a pump system, a valve modular, a load modular, and some pressure and flow sensors.

As shown in Fig. 6, the variable pump provides the flow of the total system. Its flow rate can be adjusted by adjusting the motor speed. There is a hydraulic accumulator connected to the outlet of the pump to stabilize the system pressure. When the fluid flows through flow meter, the total flow rate is measured.

The valve modular with micro-displacement control device is shown in Fig. 6, and its geometric structure (Fig. 1) has been modified by removing the spring of the valve spool and the pilot port as well as by adding a screw-transmission device axially connected to the valve spool, as shown in Fig. 7. Moreover, as the subject of this study is the fluid path P–B, all the other valve connections are bolted besides connection P, connection B, and connection C. The spool can stop at any position within the stroke due to the self-locking thread, which controls the valve opening. The axial displacement of the valve spool can be calculated with the scale value on the end

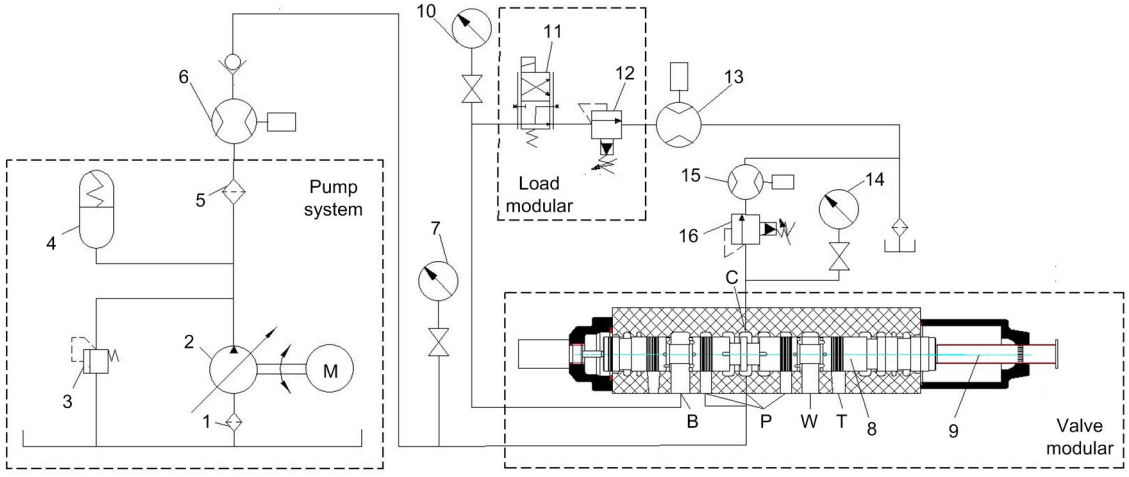

1. filter;
2. variable pump;
3. safety valve;
4. hydraulic accumulator;
5. filter;
6. flow meter;
7. pressure gauge;
8. test valve;
9. micro-displacement device;
10. pressure gauge;
11. proportional servo valve;
12. proportional relief valve;
13. flow meter;
14. pressure gauge;
15. flow meter;
16. proportional relief valve

Fig. 6 Sketch of the test bench

cover and the pitch during feeding, and a constant flow is provided by the variable pump shown in Fig. 6.

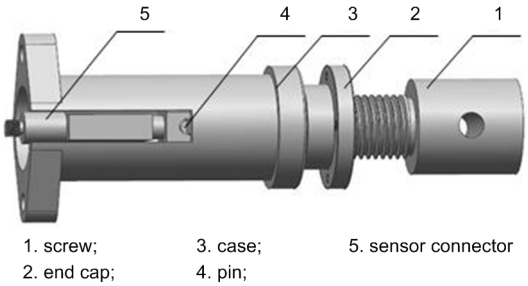

Fig. 7 Micro-displacement device

In particular, the load modular system includes the proportional servo valve and the proportional relief valve in Fig. 6, which are connected in series. Therefore, when fluid flows through these two valves, a resultant pressure is placed on the upstream port, so that a set load is constructed. Since these two valves have dynamic-response characteristics, the proportional servo valve is mainly used to simulate a high-frequency load of 5–12 Hz while the proportional relief valve is used for the lower frequency of 0–5 Hz. Therefore, during the whole process of the experiment, the proportional servo valve is kept fully opened and the outlet pressure of fluid path P–B is controlled by adjusting the proportional relief valve. Proportional servo valve installed in the test bench is for further use to study the dynamic characteristics of the valve.

The flow rate of fluid path P–B is obtained by using the flow meter shown in Fig. 6. As shown in Fig. 6, pressure gauge 7 measures the pressure at the inlet, and the outlet pressure is obtained by pressure gauge 10. In addition, the pressure differences between the inlet and outlet of fluid path P–B for different flow rates can be measured through the path when the valve is at a certain typical opening. The bench is automatically controlled using the LabVIEW program.

Fig. 8 shows the throttling test of a prototype valve. Here, the system pressure is set to 30 MPa through safety valve in Fig. 6, and the flow rate and outlet pressure are the same as the setting of the CFD simulation. Throttling tests of three openings (2.5, 3.5, and 4.5 mm) with different flow rates are carried out, as shown in Fig. 10, and the temperature during the whole test process is roughly (40±5) °C.

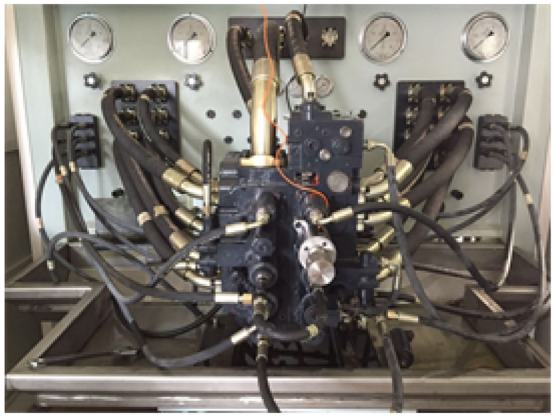

Fig. 8 Physical picture of throttling test

3.3 Results of CFD simulation and throttling test

Fig. 9 shows the CFD simulation results when the opening is x=2.5 mm. The streamline shown in Fig. 9a illustrates the chaotic and turbulent conditions of the fluids, as well as the coupling condition of the throttling grooves. Consequently, the traditional flow-coefficient formula for a thin-plate orifice is unsuitable for describing the present situation. For the opening at x=2.5 mm, Fig. 9b presents the pressure distribution, Fig. 9c presents the pressure distribution on the horizontal and vertical planes, and Fig. 9d presents the velocity distribution on the horizontal and vertical planes.

Fig. 10 shows the test and simulation results. The maximum error, which is the test value minus the numerical value, is 0.05 MPa occurring when the opening x=2.5 mm and the flow rate is 49.5 L/min. The error percentage (which equals $|(V_S-V_T)/V_T|\times 100\%$, where V_S is the numerical value and V_T is the test value) is 6.21%. All error percentages in the other cases studied are less than 7.02%. Above all, although there is some difference among the experimental and numerical curves, the throttling characteristics based on different valve openings (i.e. the differential pressure versus flow rate curves) have almost consistent trends. Accordingly, the simulation reflects the throttling effect of true working conditions. As the flow rate increases, the pressure difference between the inlet and outlet increases significantly. This trend varies with different valve openings.

Furthermore, there are some differences among the experimental and numerical curves. The differential pressures of CFD are smaller than the experimental ones because there are some leakages and pressure losses in the pipeline during the process of experiments and these cause a higher differential pressure than that in the CFD simulation. Therefore, when the outlet pressure of numerical model is set as same as the corresponding experimental one, the corresponding inlet pressure of the numerical model is smaller than that in the experimental one. With the flow rates increasing, the differences between the experimental and numerical curves, which are at the same opening, become larger because the leakages and pressure losses become larger.

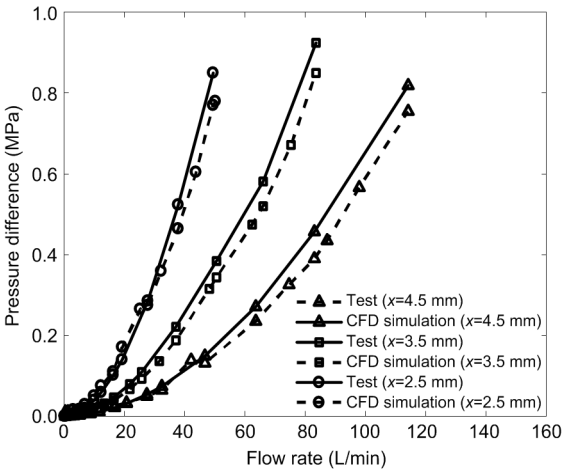

Fig. 10 Results of the CFD simulation and test

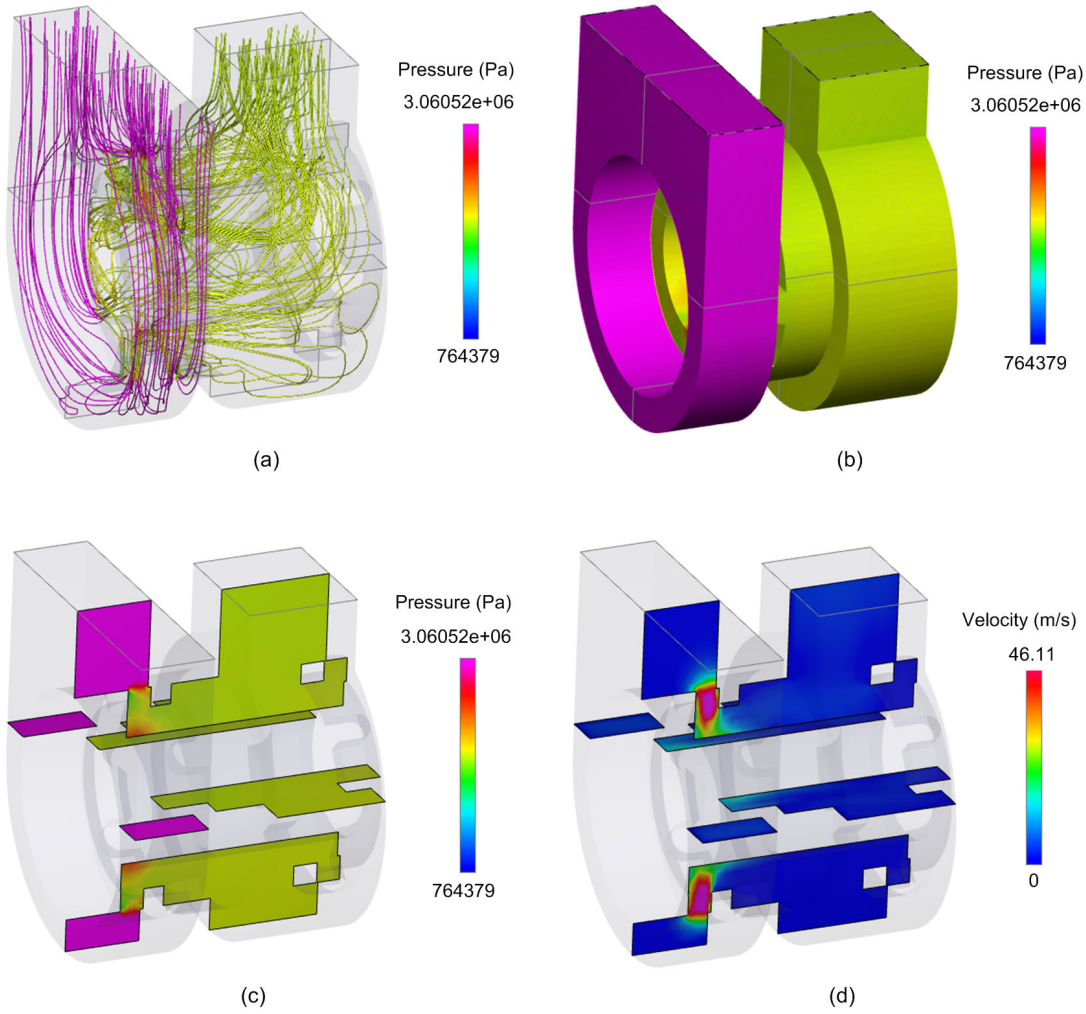

Fig. 9 CFD results of contours when the opening x=2.5 mm

(a) Streamline through the coupling grooves and pressure distribution in the chamber; (b) Pressure distribution; (c) Pressure distribution on horizontal and vertical planes; (d) Velocity distribution on horizontal and vertical planes

4 Saturation-limit model

4.1 Expressing the saturation limit

The differential pressure versus flow rate curves in Fig. 10 can be approximated as a quadratic function; as the curves pass through the coordinate origin, they can be assumed to be

$$\Delta P = aQ^2 + bQ, \tag{4}$$

where a and b are constant coefficients (Ye et al., 2014). Using Eq. (2), we obtain the following:

$$\Delta P = \frac{\rho Q^2}{2A^2 C_{\mathrm{d}}^2}. \tag{5}$$

When $c=\rho/(2A^2)$ is set, Eq. (4) can be simplified by substituting Eq. (5):

$$C_{\mathrm{d}}^2 = \frac{cQ}{aQ+b}. \tag{6}$$

Eq. (6) expresses the relationship between the flow coefficient and flow rate under the assumption of Eq. (4). However, the flow rate can only be used for describing the fluid volume per unit time, indicating that it cannot represent the flow state of the fluid. Accordingly, it is difficult to explain the mechanism behind the flow coefficient changing based on changing fluid boundaries. Therefore, the Reynolds number Re, a parameter that can be used to represent flow state, is introduced in Eq. (7) (White, 1999). Thus, we can obtain

$$Re = \frac{d_{\mathrm{H}} v}{\upsilon}, \tag{7}$$

where d_{H} is the hydraulic diameter (White, 1999), which is calculated using $d_{\mathrm{H}}=4A/\chi$. Here, χ is the all-round length of the throttling surface. v is the average flow velocity ($v=Q/A$); υ is the kinematic viscosity ($\upsilon=\mu/\rho$, where μ is the dynamic viscosity). On form converting within Eq. (7), the relationship between the Reynolds number and discharge flow can be expressed as

$$Q = kRe, \tag{8}$$

where $k=A\upsilon/d_{\mathrm{H}}$, which is determined by the structure parameters and properties of the fluid. After substituting Eq. (8) into Eq. (6), a positive value is taken as C_{d}. Thus, we can obtain

$$C_{\mathrm{d}} = \sqrt{\frac{cRe}{a\left(Re + \dfrac{b}{ak}\right)}}. \tag{9}$$

When $C_{\mathrm{dt}}=(c/a)^{1/2}$ and $k_{\mathrm{c}}=b/(ak)$, Eq. (9) can be expressed as

$$C_{\mathrm{d}} = C_{\mathrm{dt}}\sqrt{\frac{Re}{Re+k_{\mathrm{c}}}}. \tag{10}$$

Indeed, C_{dt} and k_{c} are constant when the throttling structure is definite. The relationship between the flow coefficient and Reynolds number can be expressed by Eq. (10), which also expresses the relationship between the throttling characteristics and the flow state of the fluid. Here, C_{dt} is the limit value of the flow coefficient, and k_{c} is defined as the saturation limit, which can be used to measure the degree to which the flow coefficient approaches the limit. Based on Eq. (10) (Pan et al., 2011), we can obtain

$$\lim_{Re\to\infty}\sqrt{\frac{Re}{Re+k_{\mathrm{c}}}} = 1. \tag{11}$$

In essence, if $Re \gg k_{\mathrm{c}}$, then $C_{\mathrm{d}} \approx C_{\mathrm{dt}}$. Based on Eq. (10), the Reynolds number is small with a non-saturated flow for the definite throttling structure; simultaneously, the flow coefficient correlates with the Reynolds number. Furthermore, a large Reynolds number can be obtained with a saturated flow; meanwhile, the flow coefficient is stable and has a weak correlation with the Reynolds number.

4.2 Fitting the flow-coefficient expression

Eq. (10) is derived from the assumptions of Eq. (4). Since the derivation process is reversible, its verification of accuracy is also reversible. As Eq. (10) has a visible physical meaning, its model fitting and error analysis are conducted with the CFD simulation results.

Simulation models of different openings are established in accordance with the dimensions of the real throttling groove. In the meantime, a wide range of flow rate values is set in order to represent variations in the Reynolds number. Eq. (10) is adopted to carry out curve fitting with respect to the simulation results for C_{dt} and k_c, whilst the evaluation function is generated using the least-squares method. The simulation results and fitted curve when the valve opening is 2.5 mm are presented in Fig. 11. Indeed, they are consistent with the results of Borghi et al. (2005) and Ye et al. (2014). Note that the abscissa is set as $Re^{1/2}$ for optimal observation.

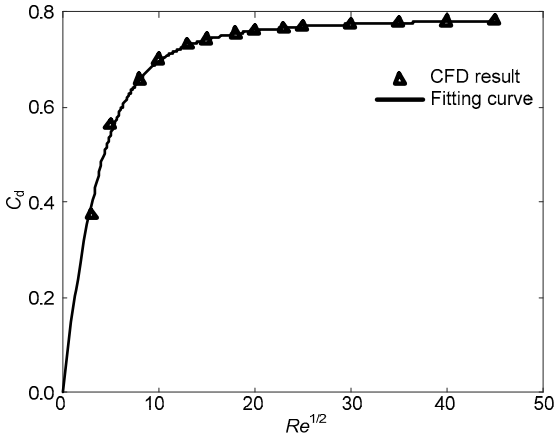

Fig. 11 Fitting curve of C_d based on the simulation results when the opening x=2.5 mm

From Fig. 11, it is evident that the fitted curve is in accordance with the simulation trend. R^2 is 0.9966, which suggests that the fit is accurate. Inlet flow rates are set based on the openings for the purpose of simulation. By adopting the same fitting method, the obtained parameters C_{dt} and k_c are shown in Fig. 12. The minimum value of R^2 is 0.9922, indicating that the model is accurate in expressing the mechanism behind the flow coefficient varying with the Reynolds number.

According to the variation law of C_{dt} and k_c in the process of increasing the openings in Fig. 12, C_{dt} first shows an increasing trend and then a decreasing one, whilst k_c shows an increasing trend. When the valve opening is relatively large (i.e. the flow area is large), C_{dt} reduces and a large Reynolds number is required for the flow coefficient to reach the limit. In general, in engineering practices, the flow coefficient is taken as the limit value. Therefore, we should determine the applied condition so that no significant error will be caused by such an approximation. Indeed, this condition can be quantitatively evaluated by the model in question. When $C_d=\alpha C_{dt}$ and $\alpha\in(0, 1)$ are set and substituted into Eq. (10), which means that α is characterisation of the allowance error when $C_d=C_{dt}$, we can obtain

$$Re=\frac{k_c\alpha^2}{1-\alpha^2}. \tag{12}$$

For instance, when the valve is in a fully open state, k_c=55.88, α=0.98, and Q=77.88 L/min are obtained using Eqs. (8) and (12) as parameters of the groove structure. This means that the flow coefficient can be set as the limit value of C_{dt} when the allowance error is 2% and the inlet flow rate is greater than 77.88 L/min at the current opening.

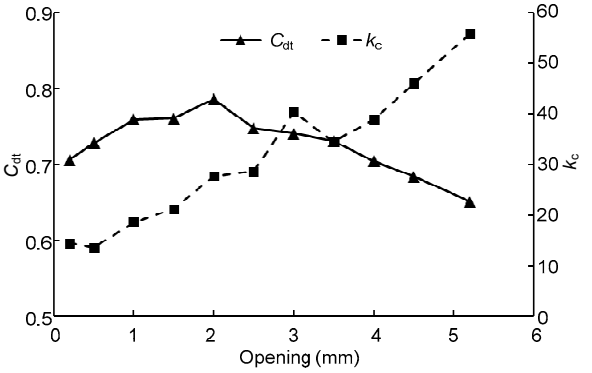

Fig. 12 Fitting parameters of C_{dt} and k_c for all the openings

5 Expression model of the flow coefficient

5.1 Structural variable space

The relationship between the flow coefficient and Reynolds number at different openings has been studied based on the throttling-groove structures previously mentioned in this paper. However, the structure of the throttling groove is designed in line with external working conditions and with a large degree of freedom for practical applications. Hence, it is necessary to study the variation law of the limit value C_{dt} with respect to the flow coefficient of different structures. The limit value can be expressed as

$$C_{\mathrm{dt}} = \Psi(\boldsymbol{L}, x), \tag{13}$$

where Ψ is the mapping relationship between C_{dt} and structural variable $\boldsymbol{L}$ as well as valve opening x.

In order to establish the throttling characteristic model in the structural variable space of the grooves, a combination of throttling grooves is required. Extending from the actual prototype structure, three typical grooves are used: O-shape, U-shape, and C-shape. It should be noted from Fig. 13 that the bottom arc of the U-shape is a semi-circle and that each structural profile is projected on the same plane. Meanwhile, the key dimensions of each groove are regarded as variables, as shown in Fig. 13. Specifically, the left end is the shoulder of the valve spool, and the valve opening is measured from the right end-point to the left. The circumferential distribution of each groove is shown in Fig. 13.

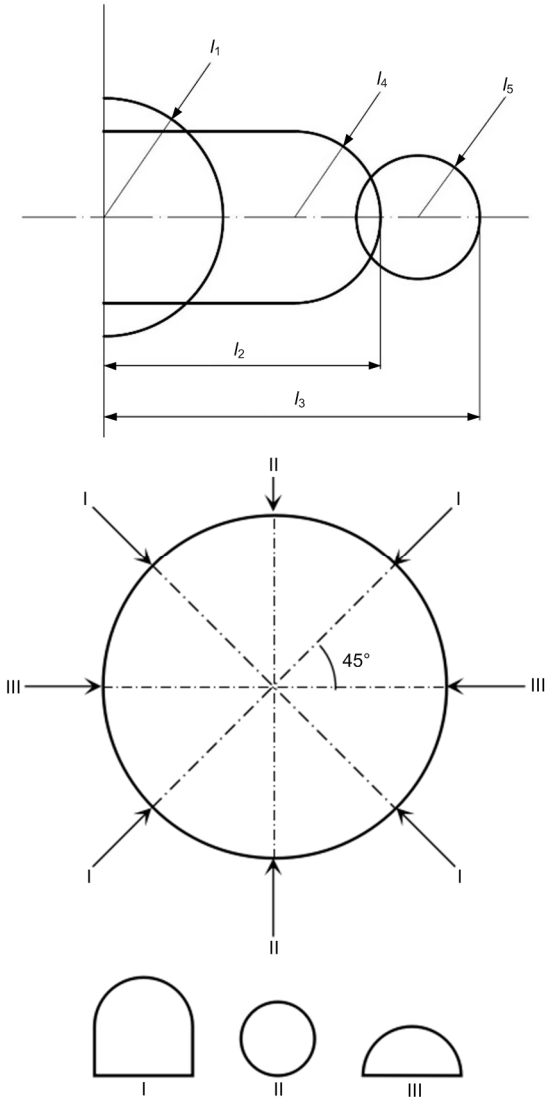

Fig. 13 Design variables and circumferential distribution of the grooves

Other assumptions include the following: (1) the number of throttling grooves does not change, specifically two O-shape grooves, four U-shape grooves, and two C-shape grooves, which are symmetrically distributed on the circumference of the valve spool, as shown in Fig. 13; (2) the structure of the valve body, the diameter of the outer circumference of the valve spool, and the groove structure of the inner ring (Fig. 3) do not change. On this basis, a 5D variable space with the combined variable $\boldsymbol{L}=\{l_1, l_2, l_3, l_4, l_5\}^{\mathrm{T}}$ of the throttling structure is established, which is used to represent a collection formed by a similar structure under different dimensional combinations.

Next, in order to reduce the number of required calculations, the orthogonal approach is utilized to extract appropriate test samples from the variable space. The principle that should be followed for determining the upper and lower boundaries of each variable is presented as follows: (1) with the dimension of a real structure of the prototype as the baseline, the boundary value should be varied within 40% of the upper and lower limits; (2) the grooves starting the throttling work are O-shape→U-shape→C-shape in sequence in the opening process of the valve; (3) the diameter of the spool should remain consistent at 18.5 mm. Orthogonal design samples in Table 1 can be obtained by taking four-level combinations from each variable with the orthogonal approach, whilst the real parameters of the prototype are shown in Table 1. The prototype is not used for establishing a model but for the purpose of verification.

5.2 Simulation analysis

CFD simulation models have been established separately for the test samples obtained in Table 1. The principle for determining the valve opening of each sample is as follows: (1) distribute over the whole stroke as evenly as possible; (2) reflect the combined features (the number and the relative position) of the throttling grooves as much as possible. The test is designed to obtain the variation law of the structural parameters corresponding to C_{dt}. Thus, the flow rate is set as saturated at the inlet of the CFD simulation. Flow coefficients calculated with each

model should be close to the limit value. They are regarded as the limit value C_{dt} in the following paragraphs. Thereafter, the k_c values of the fully opened model are calculated with the aim of expressing the conditions of the flow coefficient when the flow rate tends to the limit and checking the effective setting of the simulated flow rate.

Fig. 14 shows the results of these simulations; the trend is consistent with the results of previous research (Posa et al., 2013). As we can observe, the law of flow coefficients of each sample varies with an increase in the opening. Accordingly, it is clear that the flow coefficients are constant at the beginning of the valve opening for each sample. Indeed, only a small section of the arc areas with respect to the O-shape grooves is involved in the throttling work. With a small region, the radius of the circle has a small influence on this area. Therefore, similar results can be obtained by different samples. Moreover, it is evident that the trends for the flow coefficients of all samples increase at first and then decrease with peak values differing across a small range. Indeed, these trends are influenced by complex variations in throttling structure with respect to the valve opening process. In addition, the flow-coefficient variations tend to be linear with the opening varying at the rear section. Flow coefficients of each sample vary significantly when the valve is almost fully open. This is due to the impact caused by the large and linearly increased flow area of the rear section, indicating that the flow coefficient is significantly correlated with the flow area when the valve is fully open. Finally, the maximum value of the flow coefficient during opening is approximately at the center of the O-shape groove. If there are other grooves or structures for the throttling simulation, then the maximum point will

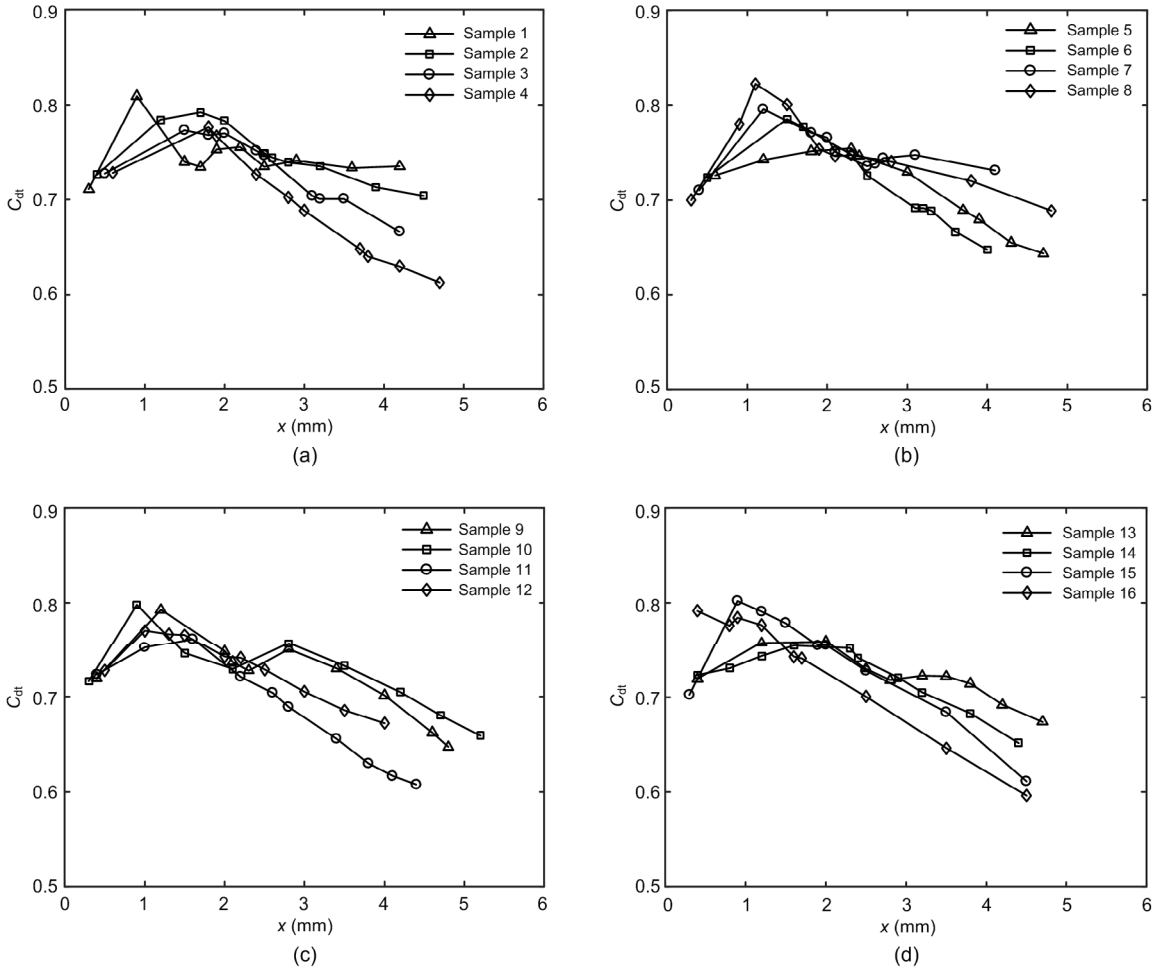

Fig. 14 Results of simulations for orthogonal samples 1–4 (a), 5–8 (b), 9–12 (c), and 13–16 (d)

shift on the horizontal axis due to the coupling influence associated with different structures.

The statistical results are provided in Table 2. Since continuous transition with respect to the simulations cannot be achieved with the valve open, the minimum opening step of the valve was set from 0.3 mm to 0.6 mm (sample 16 should be eliminated for the reason that other structures besides O-shape are involved in the throttling at the minimum opening). Accordingly, the maximum flow coefficient for each sample was recorded. The simulation results may deviate from actual values since the valve opening is not continuous. Overall, the effectiveness of the conclusions drawn above can still be shown by the statistical results. When the valve is fully open, the experiment is conducted with respect to the flow areas and flow coefficients of all samples based on Eq. (3), as shown in Fig. 15. Since R^2=0.9524, the model has a significant linear relationship.

Table 2 Statistical results of samples

Statistical parameter	C_{dt}	
	Min-opening in simulation	Maximum value
Mean value	0.7191	0.7837
Standard deviation	0.0089	0.0196
Percentage deviation (%)	1.24	2.50

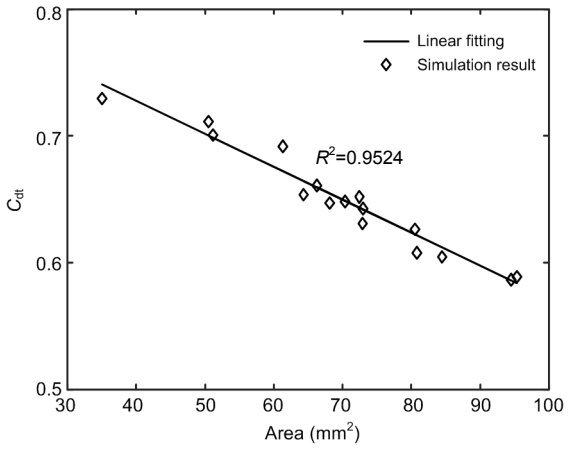

Fig. 15 Fitting curve of C_{dt} with samples fully opened

The saturation limit k_c obtained by fitting the simulation results of the test samples with a full opening is shown in Fig. 16. Although it is difficult to determine a significant variation law, it can be inferred from Fig. 12 that k_c at the full opening of each sample is larger than that at the small opening. Based on this value, the degree to which the flow coefficient approaches the limit can be evaluated. Accordingly, it can be shown that the inlet flow rates used in the simulation ensure that the flow coefficients are above 98% of the limit value, indicating that the tests and conclusions conducted in this section are reliable.

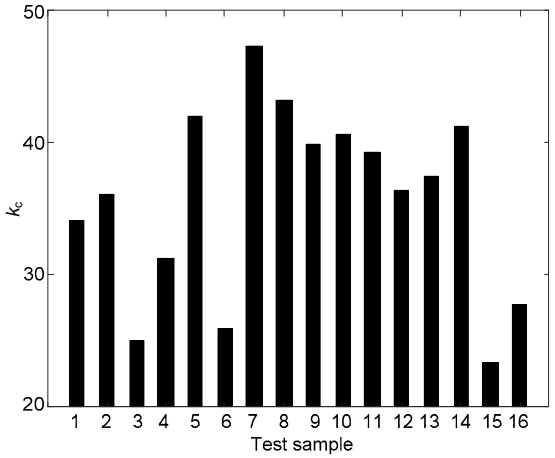

Fig. 16 k_c with samples fully opened

5.3 Approximate model for flow coefficient

In the field of spool valves, elements, such as the throttling characteristics of design variables, should be rapidly calculated in engineering practice. An approximate expression model is established for the flow coefficient within the finite variable space based on the results from the orthogonal tests, and illustrates the variation law of the flow coefficient corresponding to the structure of the throttling grooves. It should be noted that the finite variable space is the range restricted by the variable space in Section 4.1. Moreover, the upper and lower boundaries of each variable are the same as those in Table 1.

The limit value C_{dt} of the flow coefficient is set as y, which is a dependent variable. Since the influence of the variations in the Reynolds number with respect to the saturated flow state is ignored, the independent variables are the structure parameter $\boldsymbol{L}$ and the valve opening x. Accordingly, the function is expressed as $y=f(\boldsymbol{L}, x)$. By analyzing Fig. 14, a three-point linear interpolation pattern can be utilized to approximate the law of the flow coefficient varying with the valve opening for a single sample. Based on this, an expression model can be established, as shown in

Fig. 17, which is determined by three-point coordinates. As a point of x=0 mm is included, there are five variables in total. In this case, an intermediate variable $\boldsymbol{T}$ between the structural parameter and the expression model is introduced: $\boldsymbol{T}=\{t_1,\ t_2,\ t_3,\ t_4,\ t_5\}^{\mathrm{T}}$. Fig. 18 shows the exact variable-mapping diagram. As a function of $\boldsymbol{L}$, $\boldsymbol{T}$ is denoted as $\boldsymbol{T}=g(\boldsymbol{L})$. The physical significance is that t_1 is the value of flow coefficient under the minimum opening, t_2 is the value of valve opening related the maximum flow coefficient in the opening process, t_3 is the maximum value of the flow coefficient in the opening process, t_4 is the opening value when the valve is fully open, and t_5 is the value of flow coefficient when the valve port is fully open. The expression model can be presented as $y=h(\boldsymbol{T},\ x)$. A specific expression model can be obtained by determining $\boldsymbol{T}=g(\boldsymbol{L})$, the Lagrangian interpolation of which can be expressed as

$$y=\begin{cases}\dfrac{x-t_2}{-t_2}t_1+\dfrac{x}{t_2}t_3, & 0<x<t_2,\\ \dfrac{x-t_4}{t_2-t_4}t_3+\dfrac{x-t_2}{t_4-t_2}t_5, & t_2\le x\le t_4.\end{cases} \tag{14}$$

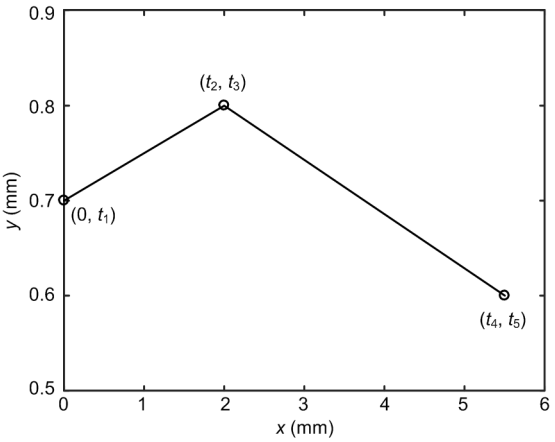

Fig. 17 Fundamental forms of the expression model

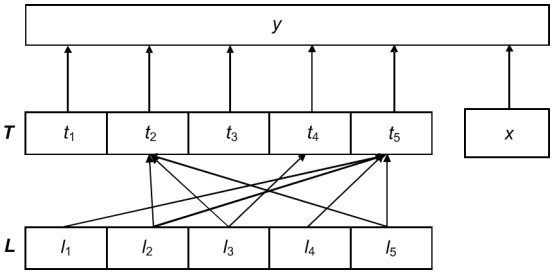

Fig. 18 Variable mapping diagram

Based on the simulation results mentioned in Section 4.2, the $\boldsymbol{T}$–$\boldsymbol{L}$ relationship can be determined. Indeed, t_1 and t_3 can be taken from Table 2 as constant values, with $t_4=l_3$. Based on the fitting results in Fig. 15, we can obtain

$$t_5=-0.0026A_{\max}(\boldsymbol{L})+0.8317, \tag{15}$$

where $A_{\max}$ is the calculation function of the throttling flow area when the valve is fully open. l_5 has the largest influence on t_2. A positive linear relationship is presented when other conditions remain constant. Next, the secondary influencing factors are l_2 and l_3, since the U-shape groove is firstly coupled with the O-shape groove, thereby presenting the coupling degree. Other factors affecting coupling, such as l_4, have low importance and can be ignored. To represent the relationships between t_2 and l_5, l_2, l_3, the assumption outlined below can be made.

$$t_2=\begin{cases}l_5, & l_3-l_2\ge l_5,\\ l_5+m\dfrac{l_3-l_2}{l_5}+n, & l_3-l_2<l_5,\end{cases} \tag{16}$$

where m and n are coefficients. In Eq. (16), when $l_3-l_2\ge l_5$, the O-shape and U-shape grooves do not have a coupling effect with respect to the maximum value of the flow coefficient. Moreover, t_2 is set as the radius of the O-shape groove; otherwise, $(l_3-l_2)/l_5$ is utilized to represent the coupling degree. Meanwhile, its primary term is deemed as the offset affecting t_2. Lastly, the coefficient n is added to correct the error.

Therefore, an expression model of the flow coefficient in finite variable space is obtained. As the model contains uncertain parameters (m and n), it should be calibrated with the simulated results of all orthogonal samples. Moreover, t_1 and t_3 can be deemed as constant values but indefinite in calibrating the fitting, so that the errors in the test-design results are distributed evenly. Indeed, calibrating the parameters of the expression model is an optimization process for parameters t_1, t_3, m, and n. The optimized objective function is the least-squares difference between the expression value and the CFD simulation value. To minimize the objective function, by setting certain limitations, the sequential quadratic algorithm

is adopted to solve the results. The calibration results are shown in Table 3.

Table 3 Results of the calibration

t_1	t_3	m	n
0.6940	0.7835	1.1767	−0.9799

6 Results and discussion

For verifying the credibility of the expression model, error analysis was conducted to calculate the relative error between the model and CFD simulation results for each sample under all openings. At this point, the relative error is $|C_{dt,M}-C_{dt,S}|/C_{dt,S}\times100\%$, where $C_{dt,M}$ is the model value and $C_{dt,S}$ is the CFD value. After statistically gathering the model results, as shown in Fig. 19, it is clear that the maximum value of the relative error with respect to all data points is 5.29%, suggesting that the model can accurately express the flow-coefficient variation law with respect to coupled throttling-groove structures in finite variable space.

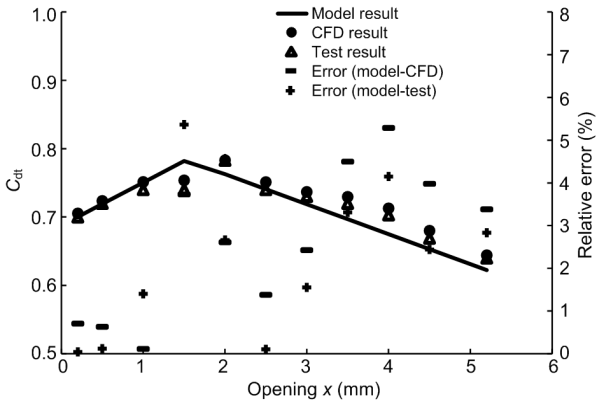

Fig. 19 Verification of model with the real structure dimension

In addition, a series of physical tests based on the real commercial prototype (Table 1) is conducted. On this basis, the test results for the real structural dimensions (Section 2) are adopted for the purpose of clarification. Indeed, the effectiveness of the results can be guaranteed, as shown in Fig. 19. The relative error between the model value and the test value is $|C_{dt,M}-C_{dt,T}|/C_{dt,T}\times100\%$, where $C_{dt,T}$ is the test value. The calculated value deviates slightly from the tested value, with a maximum relative error of about 5.34%; the total mean value of the relative error is 2.41%. This suggests that the model has a certain application value within finite variable space.

Above all, this proves the validity of this methodology with respect to approximating the flow coefficient of coupled throttling grooves accurately.

7 Conclusions and perspectives

This paper primarily presents a new methodology for accurately approximating the flow coefficient of spool valves with respect to coupled throttling grooves, based on a prototype of a typical commercial proportional–directional valve. The conclusions outlined below are drawn:

1. Based on the prototype valve, the throttling characteristics of the throttling structure, composed of three typical grooves (i.e. O-shape, U-shape, and C-shape), are examined with a test bench and a verified numerical approach. Accordingly, a concept of 'saturation limit' is proposed to deduce the flow-coefficient saturation limit of the prototype in the process. Consequently, the functional relationship between the flow coefficient and the Reynolds number was derived. The fitting results show that the model is highly effective.

2. Based on typical structures of throttling grooves, the variation law of flow coefficient corresponding to different valve openings and structures is investigated using the orthogonal-design method. Generally, the flow coefficient does not change for a small opening of the valve; moreover, the maximum value of the flow coefficient does not change very much, and the opening of the valve at the extreme value is affected by structural coupling. Indeed, the flow coefficient has a negative linear correlation with the throttling flow area when the valve is fully open.

3. A flow-coefficient expression model corresponding to variable openings and structural parameters within finite variable space is established for a throttling-groove structure. This model is shown, through error analysis and sample testing, to have a high application value.

Based on the above conclusions, further research can be conducted with respect to the aspects outlined below:

1. Since the accuracy of the established flow-coefficient model has been shown, it should be used by researchers in the spool-valve design process to optimize structural topology within proper variable space. The aim is to realize optimal structural matching with dynamic loads.

2. The test bench has the potential to expand the modular valve to realize the flow force (steady and transient) measurement acting on the valve spool, as well as the dynamic displacement of the spool with a proper dynamic frequency. Accordingly, researchers should examine the self-balancing process of the spool based on the expanded test bench when the valve is fully open.

Contributors

Xiao-lu ZHANG designed the research and built the model. An-lin WANG wrote the first draft of the manuscript. Wei CHEN and Long KUANG processed the corresponding data. Tao JIANG revised and edited the final version.

Conflict of interest

Xiao-lu ZHANG, An-lin WANG, Wei CHEN, Long KUANG, and Tao JIANG declare that they have no conflict of interest.

References

Afatsun AC, Balkan RT, 2019. A mathematical model for simulation of flow rate and chamber pressures in spool valves. *Journal of Dynamic Systems, Measurement, and Control*, 141(2):021004. https://doi.org/10.1115/1.4041300

Amirante R, Del Vescovo G, Lippolis A, 2006. Evaluation of the flow forces on an open centre directional control valve by means of a computational fluid dynamic analysis. *Energy Conversion and Management*, 47(13-14):1748-1760. https://doi.org/10.1016/j.enconman.2005.10.005

Amirante R, Distaso E, Tamburrano P, 2014a. Experimental and numerical analysis of cavitation in hydraulic proportional directional valves. *Energy Conversion and Management*, 87:208-219. https://doi.org/10.1016/j.enconman.2014.07.031

Amirante R, Catalano LA, Poloni C, et al., 2014b. Fluid-dynamic design optimization of hydraulic proportional directional valves. *Engineering Optimization*, 46(10):1295-1314. https://doi.org/10.1080/0305215X.2013.836638

Amirante R, Catalano LA, Tamburrano P, 2014c. The importance of a full 3D fluid dynamic analysis to evaluate the flow forces in a hydraulic directional proportional valve. *Engineering Computations*, 31(5):898-922. https://doi.org/10.1108/EC-09-2012-0221

Amirante R, Distaso E, Tamburrano P, 2016. Sliding spool design for reducing the actuation forces in direct operated proportional directional valves: experimental validation. *Energy Conversion and Management*, 119:399-410. https://doi.org/10.1016/j.enconman.2016.04.068

Borghi M, Cantore G, Milani M, et al., 1998. Analysis of hydraulic components using computational fluid dynamics models. *Proceedings of the Institution of Mechanical Engineers, Part C: Journal of Mechanical Engineering Science*, 212(7):619-629. https://doi.org/10.1243/0954406981521583

Borghi M, Milani M, Paoluzzi R, 2005. Influence of notch shape and number of notches on the metering characteristics of hydraulic spool valves. *International Journal of Fluid Power*, 6(2):5-18. https://doi.org/10.1080/14399776.2005.10781216

Chattopadhyay H, Kundu A, Saha BK, et al., 2012. Analysis of flow structure inside a spool type pressure-regulating valve. *Energy Conversion and Management*, 53(1):196-204. https://doi.org/10.1016/j.enconman.2011.08.021

Chen QP, Ji H, Zhu Y, et al., 2018. Proposal for optimization of spool valve flow force based on the MATLAB-AMESim-FLUENT joint simulation method. *IEEE Access*, 6:33148-33158. https://doi.org/10.1109/ACCESS.2018.2846589

Frosina E, Senatore A, Buono D, et al., 2017. A modeling approach to study the fluid-dynamic forces acting on the spool of a flow control valve. *Journal of Fluids Engineering*, 139(1):011103. https://doi.org/10.1115/1.4034418

Frosina E, Marinaro G, Senatore A, et al., 2018. Numerical and experimental investigation for the design of a directional spool valve. *Energy Procedia*, 148:274-280. https://doi.org/10.1016/j.egypro.2018.08.078

Fu X, Lu L, Ruan XD, et al., 2008. Noise properties in spool valves with cavitating flow. Proceedings of the 1st International Conference on Intelligent Robotics and Applications, p.1241-1249. https://doi.org/10.1007/978-3-540-88518-4_132

Hong SH, Kim KW, 2016. A new type groove for hydraulic spool valve. *Tribology International*, 103:629-640. https://doi.org/10.1016/j.triboint.2016.07.009

Hua B, Wang L, Du YF, et al., 2018. Design and experiment on integrated proportional control valve of automatic steering system. *IFAC-PapersOnLine*, 51(17):389-396. https://doi.org/10.1016/j.ifacol.2018.08.190

Jin ZJ, Qiu C, Jiang CH, et al., 2020. Effect of valve core shapes on cavitation flow through a sleeve regulating valve. *Journal of Zhejiang University-SCIENCE A (Applied Physics & Engineering)*, 21(1):1-14. https://doi.org/10.1631/jzus.A1900528

Lisowski E, Rajda J, 2013. CFD analysis of pressure loss during flow by hydraulic directional control valve

constructed from logic valves. *Energy Conversion and Management*, 65:285-291. https://doi.org/10.1016/j.enconman.2012.08.015

Lisowski E, Filo G, 2016. CFD analysis of the characteristics of a proportional flow control valve with an innovative opening shape. *Energy Conversion and Management*, 123:15-28. https://doi.org/10.1016/j.enconman.2016.06.025

Lisowski E, Filo G, 2017. Analysis of a proportional control valve flow coefficient with the usage of a CFD method. *Flow Measurement and Instrumentation*, 53:269-278. https://doi.org/10.1016/j.flowmeasinst.2016.12.009

Lisowski E, Filo G, Rajda J, 2015. Pressure compensation using flow forces in a multi-section proportional directional control valve. *Energy Conversion and Management*, 103:1052-1064. https://doi.org/10.1016/j.enconman.2015.07.038

Lisowski E, Filo G, Rajda J, 2018. Analysis of flow forces in the initial phase of throttle gap opening in a proportional control valve. *Flow Measurement and Instrumentation*, 59:157-167. https://doi.org/10.1016/j.flowmeasinst.2017.12.011

Lu ZY, Zhang JH, Xu B, et al., 2019. Deadzone compensation control based on detection of micro flow rate in pilot stage of proportional directional valve. *ISA Transactions*, 94: 234-245. https://doi.org/10.1016/j.isatra.2019.03.030

Majdič F, Pezdirnik J, Kalin M, 2011. Experimental validation of the lifetime performance of a proportional 4/3 hydraulic valve operating in water. *Tribology International*, 44(12):2013-2021. https://doi.org/10.1016/j.triboint.2011.08.020

Okabe H, Tanaka Y, Watanabe A, et al., 2019. Cavitation in a spool valve for water hydraulics. *IOP Conference Series: Earth and Environmental Science*, 240(6):062029. https://doi.org/10.1088/1755-1315/240/6/062029

Palau-Salvador G, González-Altozano P, Arviza-Valverde J, 2008. Three-dimensional modeling and geometrical influence on the hydraulic performance of a control valve. *Journal of Fluids Engineering*, 130(1):011102. https://doi.org/10.1115/1.2813131

Pan XD, Wang GL, Lu ZS, 2011. Flow field simulation and a flow model of servo-valve spool valve orifice. *Energy Conversion and Management*, 52(10):3249-3256. https://doi.org/10.1016/j.enconman.2011.05.010

Posa A, Oresta P, Lippolis A, 2013. Influence of the spool velocity on the performance of a directional hydraulic valve. *International Journal of Fluid Power*, 14(3):15-25. https://doi.org/10.1080/14399776.2013.10801410

SAE (Society of Automotive Engineers), 2017. Control Valve Test Procedure, Ground Vehicle Standard J747_201711. SAE International, New York, USA. https://doi.org/10.4271/J747_201711

Simic M, Herakovic N, 2015. Reduction of the flow forces in a small hydraulic seat valve as alternative approach to improve the valve characteristics. *Energy Conversion and Management*, 89:708-718. https://doi.org/10.1016/j.enconman.2014.10.037

Srikanth C, Bhasker C, 2009. Flow analysis in valve with moving grids through CFD techniques. *Advances in Engineering Software*, 40(3):193-201. https://doi.org/10.1016/j.advengsoft.2008.04.003

Tamburrano P, Plummer AR, Distaso E, et al., 2019a. A review of direct drive proportional electrohydraulic spool valves: industrial state-of-the-art and research advancements. *Journal of Dynamic Systems, Measurement, and Control*, 141(2):020801. https://doi.org/10.1115/1.4041063

Tamburrano P, Plummer AR, Distaso E, et al., 2019b. A review of electro-hydraulic servovalve research and development. *International Journal of Fluid Power*, 20(1):53-98. https://doi.org/10.1080/14399776.2018.1537456

Valdés JR, Rodríguez JM, Javier S, et al., 2014. A methodology for the parametric modelling of the flow coefficients and flow rate in hydraulic valves. *Energy Conversion and Management*, 88:598-611. https://doi.org/10.1016/j.enconman.2014.08.057

Vanella M, Posa A, Balaras E, 2014. Adaptive mesh refinement for immersed boundary methods. *Journal of Fluids Engineering*, 136(4):040909. https://doi.org/10.1115/1.4026415

Wang AL, Kuang L, Zhang XL, 2018. A study on flow coefficient of combined throttling groove in spool valves. *Journal of Xi'an Jiaotong University*, 52(2):110-117 (in Chinese). https://doi.org/10.7652/xjtuxb201802017

Wang ZQ, Gu LY, Ji H, et al., 2014. Flow field simulation and establishment for mathematical models of flow area of spool valve with sloping U-shape notch machined by different methods. *Journal of Central South University*, 21(1):140-150. https://doi.org/10.1007/s11771-014-1925-4

White FM, 1999. Fluid Mechanics, 4th Edition. McGraw-Hill, New York, USA, p.325-381.

Wu DZ, Li SY, Wu P, 2015. CFD simulation of flow-pressure characteristics of a pressure control valve for automotive fuel supply system. *Energy Conversion and Management*, 101:658-665, https://doi.org/10.1016/j.enconman.2015.06.025

Ye Y, Yin CB, Li XD, et al., 2014. Effects of groove shape of notch on the flow characteristics of spool valve. *Energy Conversion and Management*, 86:1091-1101. https://doi.org/10.1016/j.enconman.2014.06.081

Zalogin O, Noskov A, Cherevatov A, 2018. CFD analysis of fluid flow inside the spool valve at unsteady modes. Proceedings of the Global Fluid Power Society PhD Symposium. https://doi.org/10.1109/GFPS.2018.8472361

Zhang XL, Wang AL, Tang JW, 2018. Optimal design of multi-section proportional directional valve throttle grooves

with artificial neural networks. Proceedings of the 3rd International Conference on Design, Mechanical and Material Engineering.
https://doi.org/10.1051/matecconf/201823703003

中文概要

题　目： 比例换向阀耦合节流槽的流量系数表达方法

目　的： 比例换向阀阀口节流槽的耦合节流效应使其腔内流场的流量系数存在复杂性与动态性特征。本文旨在研究比例换向阀腔内流量系数的近似表达方法，以指导其设计。

创新点： 1. 在三维流场解析与台架实验结果基本一致的基础上，推导出了比例换向阀流量系数的极限饱和度模型；2. 结合正交试验方法，构建并标定了比例换向阀有限变量空间的流量系数近似模型。

方　法： 1. 通过台架试验，验证比例换向阀三维计算流体动力学（CFD）仿真的有效性（图 9 和 10）；2. 在台架试验与仿真解析结果基本一致的前提下，引入极限饱和度概念，推导出流量系数的极限饱和度表达（公式(9)和(10)）；3. 结合现有滑阀节流槽结构形态，构建基于三种典型节流槽结构（O 型、U 型和 C 型）的设计变量空间（图 13）；4. 结合试验设计方法，构建并标定有限变量空间的流量系数近似模型（图 19）。

结　论： 1. 在台架试验与仿真解析结果基本一致的基础上，推导出了比例换向阀流量系数的极限饱和度模型；2. 通过试验设计方法，得到了比例换向阀开启过程的流量系数变化趋势，即先增后减；3. 推导和标定了比例换向阀有限变量空间的流量系数近似模型，可有效实现近似模型化表达。

关键词： 流量系数；比例换向阀；耦合节流槽；饱和流量